

Identification of 3-(piperazinylmethyl)benzofuran derivatives as novel type II CDK2 inhibitors: design, synthesis, biological evaluation, and *in silico* insights

Wagdy M. Eldehna^{a,b}, Raed M. Maklad^{b,c}, Hadia Almahli^d, Tarfah Al-Warhi^e, Eslam B. Elkaeed^f, Mohammed A. S. Abourehab^g, Hatem A. Abdel-Aziz^h and Ahmed M. El Kerdawy^{i,j}

^aSchool of Biotechnology, Badr University in Cairo, Badr City, Egypt; ^bDepartment of Pharmaceutical Chemistry, Faculty of Pharmacy, Kafrelsheikh University, Kafrelsheikh, Egypt; ^cInstitute of Drug Discovery and Development, Kafrelsheikh University, Kafrelsheikh, Egypt; ^dDepartment of Chemistry, University of Cambridge, Cambridge, UK; ^eDepartment of Chemistry, College of Science, Princess Nourah bint Abdulrahman University, Riyadh, Saudi Arabia; ^fDepartment of Pharmaceutical Sciences, College of Pharmacy, AlMaarefa University, Riyadh, Saudi Arabia; ^gDepartment of Pharmaceutics, Faculty of Pharmacy, Umm Al-Qura University, Makkah, Saudi Arabia; ^hDepartment of Applied Organic Chemistry, National Research Center, Dokki, Egypt; ⁱDepartment of Pharmaceutical Chemistry, Faculty of Pharmacy, Cairo University, Cairo, Egypt; ^jDepartment of Pharmaceutical Chemistry, School of Pharmacy, NewGiza University (NGU), Cairo, Egypt

ABSTRACT

In the current work, a hybridisation strategy was adopted between the privileged building blocks, benzofuran and piperazine, with the aim of designing novel CDK2 type II inhibitors. The hybrid structures were linked to different aromatic semicarbazide, thiosemicarbazide, or acylhydrazone tails to anchor the designed inhibitors onto the CDK2 kinase domain. The designed compounds showed promising CDK2 inhibitory activity. Compounds **9h**, **11d**, **11e** and **13c** showed potent inhibitory activity (IC₅₀ of 40.91, 41.70, 46.88, and 52.63 nM, respectively) compared to staurosporine (IC₅₀ of 56.76 nM). Moreover, benzofurans **9e**, **9h**, **11d**, and **13b** showed promising antiproliferative activities towards different cancer cell lines, and non-significant cytotoxicity on normal lung fibroblasts MRC-5 cell line. Furthermore, a cell cycle analysis as well as Annexin V-FITC apoptosis assay on Panc-1 cell line were performed. Molecular docking simulations were performed to explore the ability of target benzofurans to adopt the common binding pattern of CDK2 type II inhibitors.

ARTICLE HISTORY

Received 26 February 2022
Revised 28 March 2022
Accepted 30 March 2022

KEYWORDS

Kinase inhibitors; pancreatic cancer; molecular docking; benzofuran synthesis; apoptotic agents

1. Introduction

Cancer is a group of diseases that is featured by the uncontrolled growth, proliferation and spreading (metastasis) of atypical malignant cells, it is the second cause of death in the US following heart diseases and according to the 2020 ACS cancer facts and statistics report, it is assessed that the new cancer cases have been diagnosed in 2020 in the US are more than 1.8 million cases¹.

Protein kinases (PKs) represent an important protein family in human genome (518 proteins). It regulates key cellular functions like cell growth, proliferation, and apoptosis through the coordination of cellular functions and signals^{2–6}. PKs catalyse the transport of the terminal phosphate motif in an ATP molecule onto a hydroxyl functionality in a substrate protein (phosphorylation) exerting their cellular signalling modulation⁷. PKs are classified according to the phosphorylated amino acid in the substrate protein into tyrosine and serine/threonine kinases^{7,8}. PKs are tightly regulated, and their dysregulation results in several diseases such as cancer, neurodegenerative disorders like Alzheimer's disease, and autoimmune disorders like rheumatoid arthritis. Thus PK inhibitors are a promising tool in curbing the PKs dysregulation in such disorders^{9–12}. In oncology, protein kinases inhibitors constitute a main continuously growing category of targeted chemotherapies that is free of the traditional cancer chemotherapy

common side actions as they target the signalling pathways and microenvironment of the cancer cells with minor adverse actions on normal mammalian cells^{13–16}.

Cyclin dependent kinases (CDKs) represent a conserved group of serine/threonine PKs that are involved in several key cellular processes. CDK1, CDK2, CDK4 and CDK6 subtypes are accountable for driving orderly the cell cycle in the different phases, cell differentiation and apoptosis. Furthermore, they have a crucial role in evoking cancer cells' uncontrolled proliferation^{17–19}. Pan-CDK inhibitors showed weaknesses as anticancer agents with disappointing results in clinical trials suggesting that improving selectivity towards a certain CDK is a promising strategy for developing CDK inhibitors as potential cancer chemotherapy²⁰.

Special attention has been given to CDK2 subtype as a potential target for the management and treatment of different tumours based on its key role in many cellular processes upon binding to its cyclin A or E partners; such that its complex with cyclin E regulates S phase entry and progression, whereas its binding with cyclin A warrants continuous DNA replication as well as G2/M phase transition^{20,21}. Moreover, CDK2 has a significantly broad substrate profile being responsible for the phosphorylation of many proteins which are involved in cell cycle progression, DNA replication, histone synthesis, and centrosome duplication²⁰.

CONTACT Wagdy M. Eldehna  wagdy2000@gmail.com  Faculty of Pharmacy, Kafrelsheikh University, Kafrelsheikh, Egypt

 Supplemental data for this article can be accessed [here](#).

© 2022 The Author(s). Published by Informa UK Limited, trading as Taylor & Francis Group.

This is an Open Access article distributed under the terms of the Creative Commons Attribution License (<http://creativecommons.org/licenses/by/4.0/>), which permits unrestricted use, distribution, and reproduction in any medium, provided the original work is properly cited.

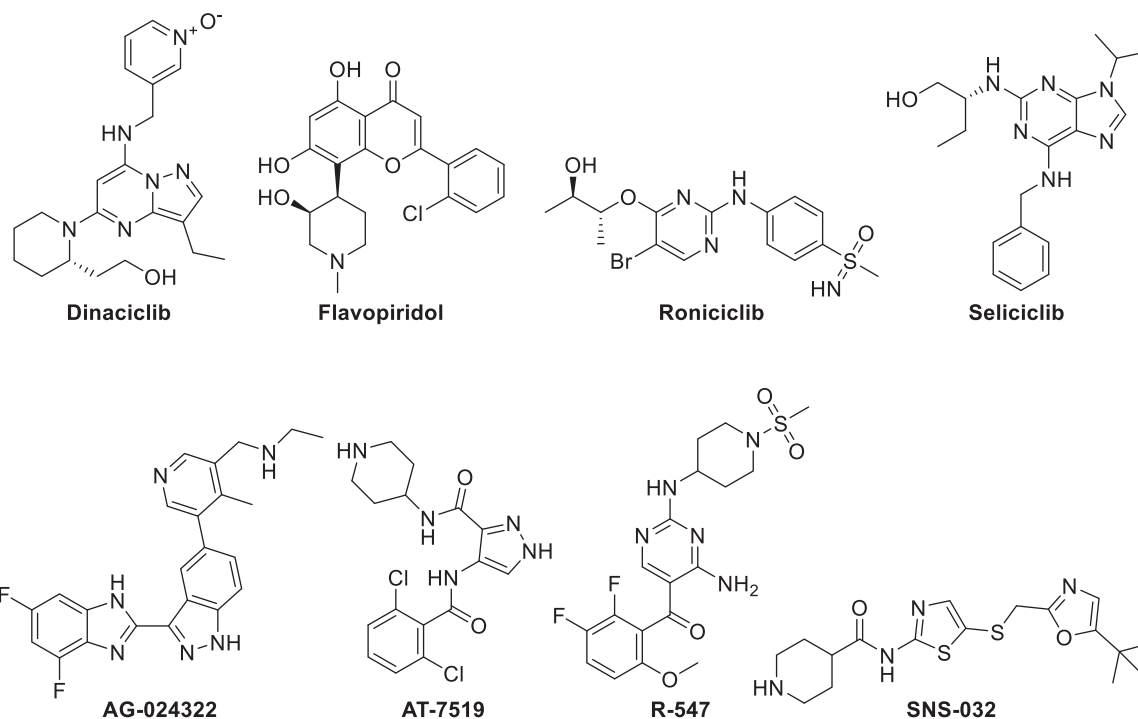


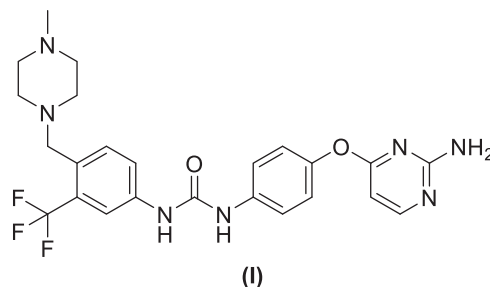
Figure 1. CDK2 inhibitors in clinical trials.

Furthermore, various cancer types showed dysregulations in CDK2 and/or its cyclin cognates such as breast cancer, endometrial, ovarian, thyroid, lung, hepatocellular carcinomas, melanoma, lymphoma, osteosarcoma, prostate, colorectal, pancreatic cancers, neuroblastoma, and BRCA deficient cancers^{20–31}. Several CDK2 inhibitors showed a promising anticancer activity, therefore, some CDK2 inhibitors were advanced through clinical trials (Figure 1)^{21,27,28,32–34}. All these facts confirm the significance of CDK2 kinase as an efficient therapeutic target for cancer management.

As a protein kinase, CDK2 can swing between active and inactive conformations due to the movement of the conserved tripeptide motif Asp-Phe-Gly (DFG) and the outward flip of the DFG loop results in the DFG-out inactive conformation^{4,35}. Accordingly, the majority of PK inhibitors can be broadly classified into type I inhibitors interacting with the DFG-in active conformation and type II inhibitors interacting with the DFG-out inactive conformation. In the general definition for the type II inhibitor pharmacophore, type II inhibitors are anchored into DFG-out conformation through hydrogen bonding in the gate area with the conserved N-lobe α C helix glutamate sidechain carboxylate and the DFG aspartate backbone NH. Moreover, type II inhibitors extend into the hydrophobic allosteric back pocket, resulted from the DFG-out flip, interacting through hydrophobic interactions with the hydrophobic side chains of the lining residues of the back pocket^{4,36–38}.

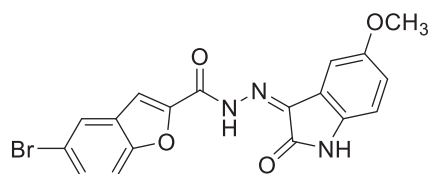
Compound I is a model CDK2 type II inhibitor interacting with the DFG-out inactive conformation. It interacts in the gate area *via* hydrogen bond interactions by its diaryl urea moiety with the α C helix Glu51 sidechain carboxylate and the DFG Asp145 backbone NH. This orientation directs the aminopyrimidine moiety from one side towards the hinge region interacting *via* H-bonding with Leu83 and from the other side, it directs the trifluoromethyl phenyl moiety into the hydrophobic allosteric back pocket interacting through hydrophobic interactions with lining amino acids. Moreover, it extends the piperazinyl moiety towards the bulk

solvent interacting through hydrogen bonding with Leu124 and His125³⁵.



Using type II inhibitors for CDK2 inhibition has several advantages over type I inhibitors, such that their extension towards the less conservative hydrophobic allosteric back pocket that enhances their affinity and selectivity^{10,37,39}. Moreover, they not only inhibit CDK2 kinase activity through ATP competition but also, they lock it in an inactive conformation which is not competent for cyclin binding, preventing the activation of CDK2³⁵. Furthermore, they possess slow off-rates (~ 10 fold slower) and prolonged target engagement and so longer residence time and duration of suppression^{4,35,40}.

Benzofuran is a privileged scaffold exhibiting numerous biological activities amongst them are analgesic, antifungal, antibacterial, anti-hyperlipidemic, antihyperglycemic, anti-inflammatory, antioxidant, antipyretic, antiviral, as well as antitumor actions^{41–44}. Benzofuran-based derivatives can exert the antitumor actions *via* several mechanisms such as the inhibition of farnesyltransferase, oestrogen receptor, human peptide deformylase, tubulin polymerisation, angiogenesis, or carbonic anhydrases^{41,45}. In addition, many benzofuran-based small molecules mediate their anticancer actions through protein kinases inhibition such as GSK-3 β ^{44,46}, mTOR signalling^{47,48}, Pim-1⁴⁹, Src kinase⁵⁰, as well as CDK2⁴⁴. Compounds II showed a potent CDK2 inhibitory activity with IC₅₀ of 52.75 nM inducing cell cycle arrest of MCF-7 breast cancer cells within the G2/M phase causing cell apoptosis⁴⁴.



(II)

Piperazine is another privilege heterocycle that represents a key moiety in several bioactive small molecules that show a broad spectrum of biological activities^{51–56}. Piperazine derivatives show antibacterial, anticonvulsant, antidepressant, antifungal, antimalarial, antimycobacterial, anthelmintic, antiviral, cardio protecting, as well as anticancer activities^{55,56}. They were reported to exert their anticancer activities through diverse mechanisms such as production of reactive oxygen species (ROS) and decreasing of c-FLIP⁵⁷, Lysine-specific histone demethylase 1A (LSD1) inhibition⁵⁸, ROS-mediated RhoB expression through the upregulation of c-Abl, as well as the activation of p38 MAPK/ATF-2⁵⁹, dual inhibition of REV-ERB β and autophagy⁶⁰, ribonucleotide reductase (RR) and HDAC inhibition⁶¹, depolarisation of mitochondrial membrane potential⁶², chemokine receptor (CCR5) antagonism⁶³, DNA intercalation⁶⁴, smoothened antagonism^{65,66}, stearyl-CoA desaturase inhibition⁶⁷, Bcl-2/Bcl-xl inhibition⁶⁸, and PARP1 inhibition⁶⁹. In addition, one of the main mechanisms for piperazine derivatives anticancer activity is kinase inhibition such as anaplastic lymphoma kinase (ALK)⁷⁰, BCR-Abl⁷¹, RET kinase⁷², epidermal growth factor receptor (EGFR)⁷³, vascular epithelial growth factor receptor 2 (VEGFR-2)⁷⁴, focal adhesion kinase (FAK)⁷⁵, as well as CDKs family, CDK2^{35,51,76}, CDK4/6⁷⁷, and CDK9⁷⁶ (Figure 2).

Despite of the forementioned type II advantages, most of the CDK2 inhibitors discovery campaigns focus on designing type I inhibitors. In the current work, a hybridisation strategy was adopted between the privileged building blocks, benzofuran and piperazine,

with the aim of designing novel CDK2 type II inhibitors. The hybrid structures were linked to different aromatic thiosemicarbazide, semicarbazide, or acylhydrazone tails to anchor the designed inhibitors onto the CDK2 DFG-out conformation in the gate area through hydrogen bonding to the conserved α C glutamate (α C-Glu51) and the aspartate of the DFG motif (DFG-Asp154) (Figure 3).

Different aromatic moieties were used in the tail part to study their effect on the binding affinities and the kinase inhibitory activities. The newly synthesised hybrids were then tested for their CDK2 inhibitory activity and cytotoxic activity using pancreatic cancer (Panc-1), breast cancer (MCF-7), and lung carcinoma (A549) cell lines. Moreover, their safety was assessed using human lung fibroblast normal cell line (MRC-5). To confirm their mode of action, the effect of representative compounds **9h** and **11d** on cell cycle progression were also investigated. Finally, molecular docking simulations were carried out to confirm their binding mode and to rationalise their structure activity relationships (SARs).

2. Results and discussion

2.1. Chemistry

The retrosynthetic analyses for all target 3-(piperazinylmethyl)benzofurans (**9**, **11**, **13**, **15** and **17**) have led to a consensus of utilising the hydrazide **7** as a building block. An appropriate synthesis of the benzofuran cyclisation step is outlined in Scheme 1. Firstly, an O-C2 bond was formed in the newly emerging furan ring *via* utilising an S_N2 reaction of ethyl α -chloroacetate **2** with sodium phenoxide nucleophile. Then, a C3-C4 bond was formed to furnish the desired benzo[*b*]furan derivative **4** *via* a dehydration step carried out on the α -phenoxy- β -ketoester **3** using sulphuric acid at mild conditions. After that, the 3-methyl group of compound **4** was activated for further nucleophilic substitution reaction by introducing bromine atom

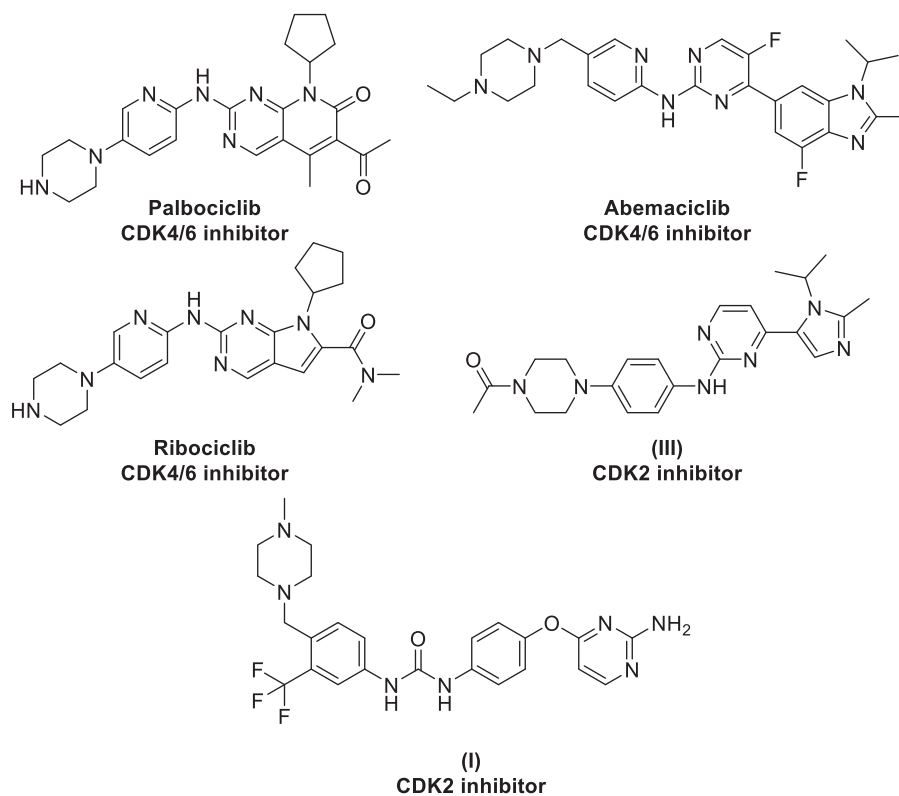


Figure 2. Representative piperazine derivatives with CDKs inhibitory activity.

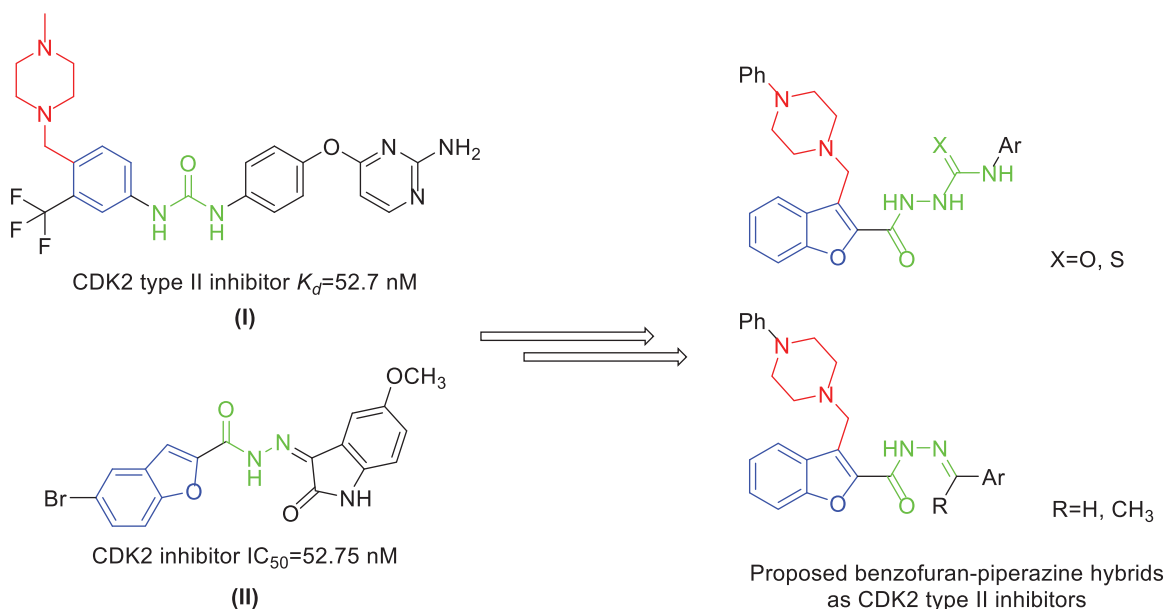
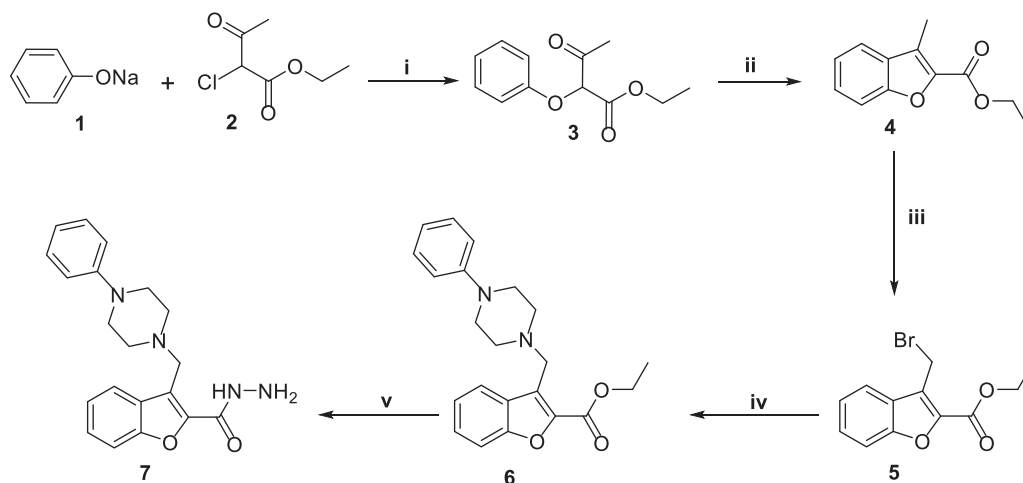


Figure 3. The design strategy of the novel benzofuran-piperazine hybrids as CDK2 type II inhibitors.



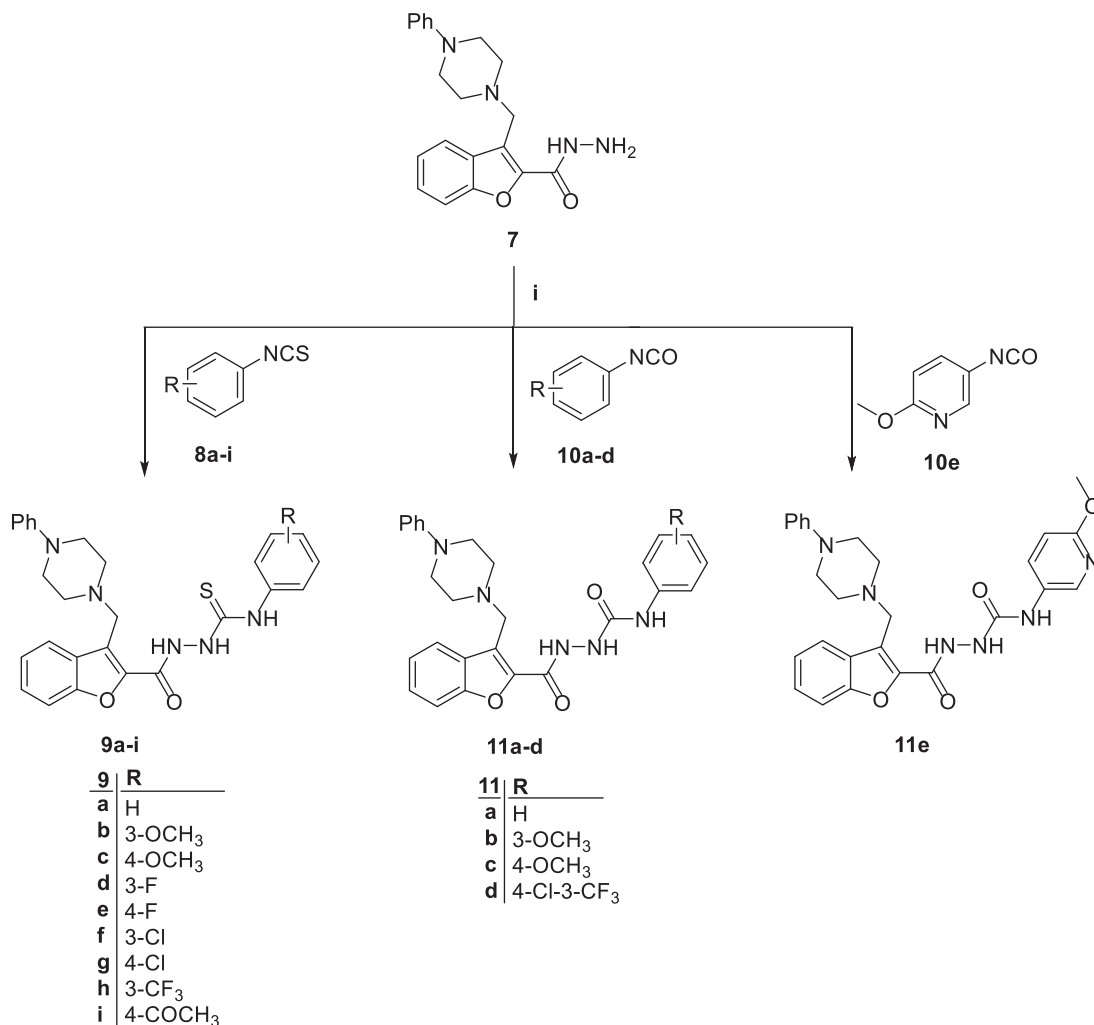
Scheme 1. Reagent and conditions: (i) Toluene, reflux 4 h; (ii) Sulphuric acid, stirring 2 h (0–5 °C); (iii) NBS, CCl₄, reflux 3 h; (iv) *N*-phenylpiperazine, acetone, K₂CO₃, KI, reflux 4 h; (v) 99% NH₂NH₂·H₂O, ethyl alcohol, reflux 4 h.

using *N*-bromosuccinimide reagent to afford the 3-(bromomethyl)-benzofuran derivative **5**. Compound **5** was then subjected to an S_N2 reaction with *N*-phenylpiperazine in refluxing acetone using anhydrous potassium carbonate as a base to afford the *N*-phenylpiperazinyl substituted benzofuran ester **6**. It's noteworthy mentioning the catalytic role of potassium iodide, acting as a nucleophilic assistant in the S_N2 mechanism which afforded a noticeable increase in the experimental reaction yield. Finally, the target hydrazide intermediate **7** was obtained *via* hydrazinolysis of the corresponding ester precursor **6** in refluxing ethanol.

Regarding the synthesis of target benzofurans **9**, **11**, **12**, **14** and **16**, the hydrazide **7** was coupled with isothiocyanates **8a-i** and isocyanates **10a-e** *via* nucleophilic addition reaction in refluxing toluene to afford the desired thiosemicarbazides **9a-i** and semicarbazides **11a-e**, respectively (Scheme 2). Analogously, the aldehydrazones **13a-c** as well as the ketohydrazones **15a,b** & **17** were prepared by a simple condensation reaction of the hydrazide **7** with the aldehydes **12a-c** and ketones **14a,b** & **16** in refluxing ethanol using weak acid catalysis (Scheme 3).

The structure of intermediates **6**, **7** as well as those of target compounds **9**, **11**, **13**, **15** and **17** were confirmed by ¹H as well as

¹³C NMR spectral analysis (see the NMR charts in the supplementary material). All of the relevant spectral data of these compounds shared some common NMR signals. These included the following ¹H NMR signals: Ar-H of C4, C7, C6 and C5 of benzofuran nucleus at δ_{ppm} around 8 (d), 7.7 (d), 7.5 (t) and 7.4 (t), respectively; Ar-H of the phenyl ring at N4 piperazine at δ_{ppm} around 7.2, 6.9 and 6.8; two sets of aliphatic Hs of piperazine ring at δ_{ppm} around 3.1 (4H) and 2.6 (4H); methylene group exocyclic to C3 benzofuran at δ_{ppm} around 4.1 (2H, s). Moreover, compound **7** was confirmed by NH hydrazide signal at δ_{ppm} 10.68; compound series **9a-i** and **11a-e** by the three NH (thio)semicarbazide singlets at δ_{ppm} around 12.2, 9.9 and 9.8; aldehydrazone series **13a-c** by the characteristic H-C=N hydrazone signal at δ_{ppm} around 8.5; compounds **15a,b** by the characteristic CH₃-C=N at δ_{ppm} around 2.5 (3H, s); and finally compound **17** by the characteristic aliphatic H signals of 3,4-dihydronaphthalen-1(2H)-ylidene moiety at δ_{ppm} 1.99–1.80 (m, 2H), 2.92–2.78 (m, 4H) in addition to the relevant aromatic ones at δ_{ppm} 8.04 (d, *J*=7.8 Hz, 1H, Ar-H at C8), 7.40–7.28 (m, overlapped signals including Ar-H at C6,7) and 7.28–7.18 (m, overlapped signals including Ar-H at C5). Finally, the Ar-H signals corresponding to the additional (substituted)phenyl



Scheme 2. Reagent and conditions: (i) Toluene, reflux 7 h.

ring hydrogens at N4 (thio)semicarbazide in benzofurans **9a-i**, **11a-e** as well as those Ar-Hs of the benzylidene moiety at N1 hydrazide in benzofurans **13a-c**, **15a,b** were characteristic for structure confirmation of these compounds (See the Experimental section for details).

Regarding ¹³C NMR spectral analysis, structures of all studied compounds were in agreement with the expected ones as confirmed by the number of ¹³C NMR signals corresponding to aliphatic, aromatic, carbonyl and/or imine carbons (see the experimental section and the [supplementary material](#)).

2.2. Biological evaluation

To validate the design strategy, assessments of the CDK2 inhibitory activity as well as the anticancer activities for the newly synthesised piperazine tethered benzofuran derivatives were carried out. The cytotoxic activity was evaluated against pancreatic cancer (Panc-1), breast cancer (MCF-7), and lung carcinoma (A549) cell lines. Moreover, the effect of the most promising compounds on the cell cycle progression was also investigated in order to confirm their mode of action.

2.2.1. Cdk2 inhibitory activity

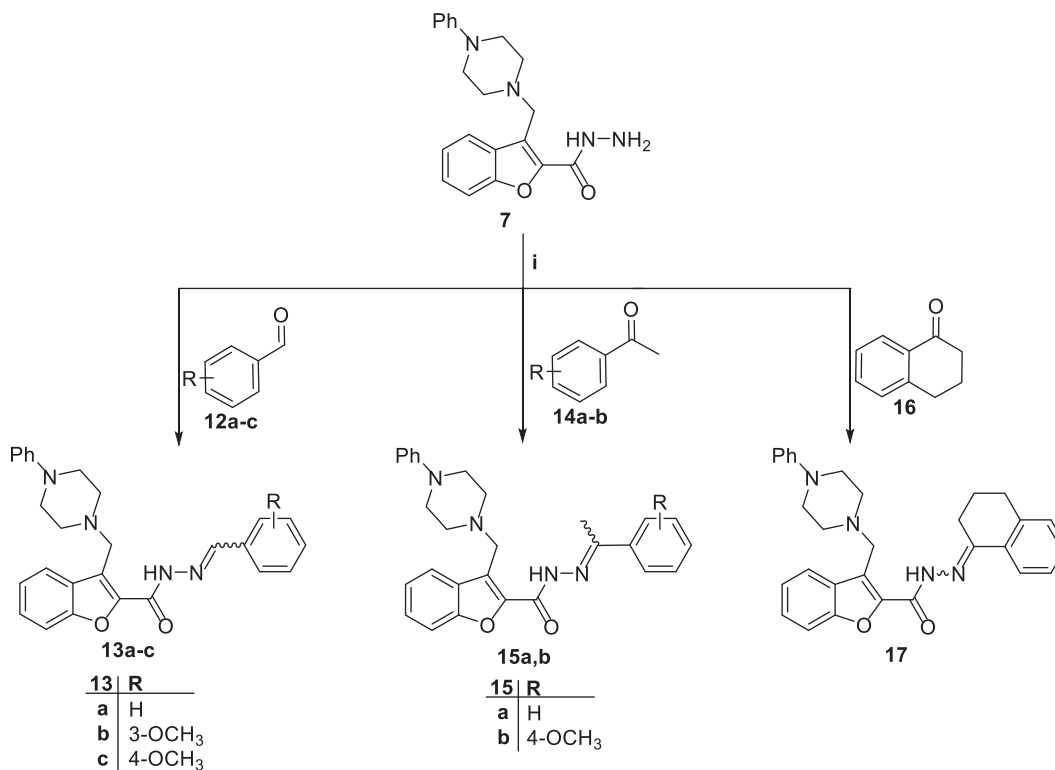
To validate the design strategy in this work which aim to the design of potent CDK2 inhibitors, the CDK2 inhibitory activity of

all the newly synthesised piperazine tethered benzofurans **9a-i**, **11a-e**, **13a-c**, **15a,b** and **17** was evaluated against staurosporine as a reference standard and IC₅₀ were calculated in nM.

The thiosemicarbazide derivatives **9a-i** showed CDK2 inhibitory concentration (IC₅₀) range of 40.91–322.1 nM. The *m*-trifluoromethyl derivative **9h** showed potent inhibitory activity relative to that of staurosporine (IC₅₀ = 40.91 vs 56.76 nM, respectively). Compounds **9b**, **9d**, **9e**, **9g** and **9i** showed comparable CDK2 inhibitory activity to that of staurosporine (the used reference standard) with IC₅₀ less than 100 nM. Compounds **9a**, **9c** and **9f** showed weak inhibitory activity compared to that of staurosporine (IC₅₀ = 322.10, 214.00 and 119.00 nM, respectively, vs 56.76 nM) (Table 1).

The semicarbazide derivative **11a-e** showed CDK2 inhibitory concentration (IC₅₀) range of 41.70–182.5 nM. The 4-Cl-3-CF₃-phenyl derivative **11d** and the pyridyl derivative **11e** showed potent inhibitory activity relative to that of staurosporine (IC₅₀ = 41.7 and 46.88 nM, respectively, vs 56.76 nM). Whereas compounds **11a-c** showed weaker CDK2 inhibitory activity relative to that of staurosporine (IC₅₀ of 137.20, 129.30 and 182.50 nM, respectively, vs 56.76 nM) (Table 1).

The acylhydrazone counterparts **13a-c**, **15a,b** and **17** showed CDK2 inhibitory concentration (IC₅₀) range of 52.63–333.17 nM. The *p*-methoxyphenyl derivative **13c** showed slightly potent inhibitory activity relative to that of staurosporine (IC₅₀ = 52.63 vs 56.76 nM, respectively). Compounds **13b** and **17** showed comparable CDK2 inhibitory impact to that of staurosporine with IC₅₀ of



Scheme 3. Reagent and conditions: (i) Absolute ethyl alcohol, acetic acid (cat.), reflux 11 h.

Table 1. Inhibitory activities of the newly synthesised benzofuran derivatives **9a-i**, **11a-e**, **13a-c**, **15a-b** and **17** against CDK2

Comp.	IC ₅₀ (nM) ^a CDK2
9a	322.10 ± 16
9b	84.92 ± 4.30
9c	214.00 ± 11
9d	77.67 ± 41
9e	64.97 ± 3.30
9f	119.00 ± 6.10
9g	69.80 ± 3.60
9h	40.91 ± 2.10
9i	89.44 ± 4.62
11a	137.20 ± 7.00
11b	129.30 ± 6.60
11c	182.50 ± 9.30
11d	41.70 ± 2.10
11e	46.88 ± 2.40
13a	151.70 ± 7.70
13b	65.63 ± 3.31
13c	52.63 ± 2.70
15a	333.10 ± 17
15b	127.10 ± 6.50
17	65.58 ± 3.30
Staurosporine	56.76 ± 2.90

^aIC₅₀ values are the mean ± SD of three separate experiments. Bold values indicate the best results.

65.63 nM and 65.58 nM, respectively. The unsubstituted phenyl derivative **13a** and the methyl acylhydrazone derivatives **15a** and **15b** showed weak inhibitory activity compared to that of staurosporine (IC₅₀ = 151.70 nM, 333.10 nM and 127.10 nM, respectively, vs 56.76 nM) (Table 1).

These results highlighted that, as planned, the designed compounds showed promising CDK2 inhibitory activity with compounds **9h**, **11d**, **11e** and **13c** showing potent inhibitory activity compared to staurosporine (the used reference standard), Table 1.

2.2.2. In vitro anti-proliferative activity

To study the antiproliferative activity of the newly synthesised piperazine tethered benzofuran derivatives **9a-i**, **11a-e**, **13a-c**, **15a,b** and **17**, their cytotoxic activity were evaluated using pancreatic cancer (Panc-1), breast cancer (MCF-7), and lung carcinoma (A549) cell lines which are known to possess CDK2 dysregulation^{20–31}.

The thiosemicarbazide derivatives **9a-i** show comparable cytotoxicity on the tested cell lines with IC₅₀ ranges of 0.94–125.85 μM, 2.92–127.65 μM and 1.71–126.89 μM against Panc-1, MCF-7, and A549 cell lines, respectively. The *m*-trifluoromethyl derivative **9h** displayed the most potent activity in this series with IC₅₀ of 0.94, 2.92 and 1.71 μM, and more potent than that of the used reference standard (cisplatin) which showed IC₅₀ of 6.98, 5.45 and 6.72 μM against Panc-1, MCF-7, and A549 cell lines, respectively. Whereas the *p*-fluoro derivative **9e** was the second most potent in this series with IC₅₀ of 3.29, 5.89 and 5.24 μM against Panc-1, MCF-7, and A549 cell lines, respectively, which is also more potent than that of cisplatin (Table 2).

Likewise, the semicarbazide derivatives **11a-e** show comparable cytotoxicity on the tested cell lines with IC₅₀ ranges of 2.22–61.45 μM, 5.57–76.93 μM and 2.99–56.95 μM against Panc-1, MCF-7, and A549 cells, respectively. The 4-Cl-3-CF₃-phenyl derivative **11d** showed the most potent cytotoxic activity in this series with IC₅₀ of 2.22, 5.57 and 2.99 μM against Panc-1, MCF-7, and A549 cell lines, respectively, that is also more potent than that of cisplatin (IC₅₀ of 6.98, 5.45 and 6.72 μM, respectively) (Table 2).

The acylhydrazone derivatives **13a-c**, **15a,b** and **17** exerted comparable cytotoxicity towards the tested cell lines displaying IC₅₀ ranges of 1.04–169.27 μM, 2.98–122.98 μM and 1.71–108.76 μM against Panc-1, MCF-7, and A549 cells. The *m*-methoxyphenyl derivative **13b** showed the most potent cytotoxic activity in this series with IC₅₀ of 1.04, 2.98 and 1.71 μM against Panc-1, MCF-7,

Table 2. Anti-proliferative activities of hybrids **9a-i**, **11a-e**, **13a-c**, **15a,b** and **17** against Panc-1, MCF-7 and A-549 cancer cell lines.

Comp.	IC ₅₀ (μM) ^a		
	Panc-1	MCF-7	A-549
9a	86.92 ± 4.17	118.49 ± 6.02	85.47 ± 6.21
9b	61.88 ± 3.48	98.49 ± 4.47	80.44 ± 4.87
9c	103.13 ± 6.21	86.63 ± 5.28	72.19 ± 5.36
9d	27.19 ± 1.87	53.89 ± 3.57	40.39 ± 2.74
9e	3.29 ± 0.20	5.89 ± 0.43	5.24 ± 0.40
9f	125.85 ± 7.06	127.41 ± 7.56	126.89 ± 7.61
9g	121.69 ± 6.34	120.65 ± 8.39	110.77 ± 6.38
9h	0.94 ± 0.10	2.92 ± 0.17	1.71 ± 0.12
9i	19.15 ± 1.27	27.33 ± 2.05	29.23 ± 2.06
11a	56.82 ± 2.94	55.88 ± 3.18	49.30 ± 3.27
11b	10.19 ± 0.86	15.19 ± 1.34	13.84 ± 1.04
11c	61.45 ± 4.52	76.93 ± 5.21	56.95 ± 2.33
11d	2.22 ± 0.13	5.57 ± 0.47	2.99 ± 0.21
11e	54.56 ± 4.22	48.70 ± 3.54	44.75 ± 4.62
13a	169.27 ± 9.41	118.40 ± 8.39	108.76 ± 7.59
13b	1.04 ± 0.08	2.98 ± 0.18	1.71 ± 0.10
13c	4.47 ± 0.29	13.64 ± 0.94	14.38 ± 1.02
15a	120.12 ± 5.77	122.98 ± 6.82	98.38 ± 5.61
15b	25.38 ± 1.70	44.35 ± 2.96	28.47 ± 1.92
17	80.40 ± 4.83	82.80 ± 5.43	58.87 ± 1.88
Cisplatin	6.98 ± 0.35	5.45 ± 0.40	6.72 ± 0.37

^aIC₅₀ values are the mean of 3 separate experiments.

Table 3. Inhibitory activities against non-tumorigenic human lung fibroblast MRC-5 cell line

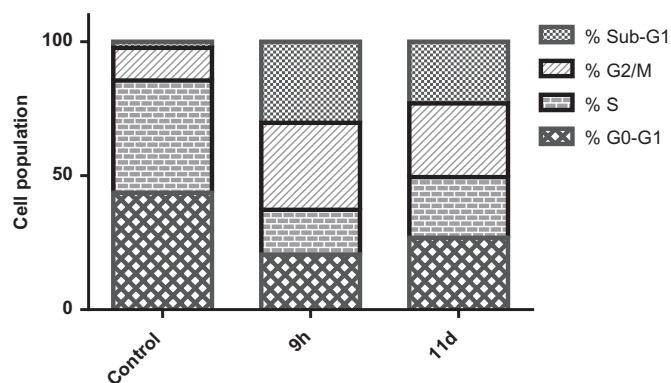
Comp.	IC ₅₀ (μM) ^a	SI ^b
	MRC-5	
9a	406 ± 21	4.75
9b	289 ± 19	3.59
9c	261 ± 20	3.62
9d	166 ± 14	4.11
9e	52 ± 3	9.92
9f	391 ± 25	3.08
9g	342 ± 30	3.09
9h	27.7 ± 1.8	16.20
9i	142 ± 11	4.86
11a	178 ± 13	3.61
11b	121 ± 10	8.74
11c	246 ± 13	4.32
11d	74 ± 5	24.75
11e	244 ± 18	5.45
13a	>500	>4.60
13b	18.1 ± 1.3	10.58
13c	121 ± 9	8.41
15a	452 ± 28	4.59
15b	160 ± 10	5.62
17	284 ± 15	4.82

^aIC₅₀ values are the mean of three separate experiments.

^bSI safety index calculated as IC₅₀ in normal lung cell/IC₅₀ in cancerous lung cells A-549.

and A549 cells, respectively, that is also more potent than that of cisplatin (IC₅₀ of 6.98, 5.45 and 6.72 μM, respectively) (Table 2). The *p*-methoxyphenyl derivative **13c** showed more potent cytotoxic activity against Panc-1 cell line than that of cisplatin (IC₅₀ of 4.47 vs 6.98 μM, respectively) (Table 2).

These results show that in the different series, each compound has comparable cytotoxic activities on the tested cancer cell lines. These results show also that compounds **9e**, **9h**, **11d**, and **13b** are the most potent antiproliferative compounds in agreement with their potent CDK2 inhibitory activity (Tables 1 and 2). Despite of its potent CDK2 inhibitory activity, compound **11e** showed moderate antiproliferative activity which could be rationalised to its poor cellular intake.

**Figure 4.** Impact of benzofurans **9h** and **11d** towards the cell cycle phases of Panc-1 cancer cells.

2.2.3. In vitro normal cell cytotoxicity

To test the safety of the newly synthesised compounds and their selectivity towards cancer cells, their cytotoxic activity was tested on non-tumorigenic human lung fibroblast MRC-5 cell line. All the tested compounds showed a high IC₅₀ on normal human lung fibroblast relative to their IC₅₀ on cancerous lung cell line A-549 with selectivity index (SI) higher than 3 folds.

The most potent compounds **9e**, **9h**, **11d**, and **13b** showed IC₅₀ on MRC-5 of 52.00, 27.70, 74.00 and 18.10 μM, respectively, which represent SI of 9.92, 16.20, 24.75 and 10.58, respectively (Table 3). These results indicate that these benzofuran derivatives are not only with promising CDK2 inhibitory effect and cytotoxicity but also with selectivity towards cancerous cells and so tolerable and safe effect on normal cells.

2.2.4. Cell cycle analysis

As previously mentioned, CDK2/cyclin E complexation regulates S phase entry and progression, whereas CDK2/cyclin A complexation permits continuous DNA replication and G2/M phase transition and progression^{24,30,78,79}. Moreover, a significant CDK2-deficient cells percentage could be arrested in the G2/M phase, in addition, cancerous cells treated with CDK2 inhibitors display an arrest within the G2/M phase^{22,80}.

In this research work, the effect of the two most efficient cell growth inhibitors **9h** and **11d** towards the progression of the cell cycle was investigated aiming to explore the cell cycle phase which could be arrested to confirm the mode of action of the target benzofurans. Panc-1 cancerous cells were incubated with the IC₅₀ dose of both benzofurans **9h** and **11d**, and the impact on the cells populations was determined within the different cell phases. Treatment of Panc-1 cells with **9h** and **11d** led to a significant decline in the cells population regarding the G0/G1 and S phases from 43.57% and 41.90%, respectively, in the control to 20.56% and 16.66%, respectively, with compound **9h** and 26.83% and 22.61%, respectively, with compound **11d** (Figure 4). This is accompanied by a significant elevation in the proportion of cells in G2/M phase with compounds **9h** and **11d** (32.46% and 27.52%, respectively) relative to the control (12.17%) with simultaneous increase in the proportion of cells in the sub-G1 phase (30.32% and 23.04%, respectively) in comparison to the control (2.36%). These results indicate that the newly synthesised compounds cause cell cycle arrest in the G2/M phase which is the main criterion of CDK2 inhibitors confirming the mode of action under investigation.

2.2.5. Annexin V-FITC (Anx V) apoptosis assay

Anx V flowcytometry assay is featured as a helpful tool to determine whether cells death is due to the physiological apoptosis or to the non-specific necrosis. In this work, the impact of the most promising benzofurans **9h** and **11d** towards Panc-1 cell apoptosis was investigated using Anx V-propidium iodide dual staining analysis in accordance with the standard protocol⁸¹.

The Anx V-based flowcytometry assay results (Figure 5) revealed that the total apoptotic cells percentage in Panc-1 cancerous cells increased upon treatment with benzofurans **9h** and **11d** from 2.41% (for the control cells) to 43.51 and 29.93%, respectively, which significantly suggest the apoptotic impact of the target 3-(piperazinylmethyl) benzofuran derivatives. In details, benzofurans **9h** and **11d** were able to elevate the percentages of the early apoptotic phases from 0.59% (for the control cells) to 5.41% and 2.64%, respectively, in addition they increased the percentages of the late apoptotic phase, from 0.32% in control to 20.99% and 15.87%, respectively. This obviously verifies that the anti-proliferative impact of the designed 3-(piperazinylmethyl) benzofuran derivatives is attributable to the physiological apoptosis and not attributable to the non-specific necrosis.

2.3. Molecular docking study and SAR

CDK2 is one of the kinases that have a considerable number of structures in the protein data bank (PDB), with more than 200 available crystal structures in the PDB co-crystallized with different inhibitors^{30,35,82}. Nearly all available crystal structures are for CDK2 protein adopting DFG-in conformation co-crystallized with type I inhibitors accommodated in the hinge region³⁵. In this molecular modelling study, one of the unique CDK2 crystal structures

adopting DFG-out conformation co-crystallized with type II inhibitor (compound **I**) has been utilised (PDB ID: 5A14)³⁵.

Firstly, self-docking for the co-crystallised ligand (compound **I**) within the CDK2 binding site was carried out to prove the molecular docking setup to be used. Self-docking validation precisely reproduced the binding mode of the co-crystallised ligand highlighting the aptness of the adopted modelling protocol for the intended molecular docking simulations. In addition, it was confirmed through the small RMSD between the docked and the co-crystallised ligand poses of 0.245 Å ($S = -16.61$ kcal/mol), and also by the capability of the accomplished docking pose to regenerate the main binding interactions achieved by the co-crystallised ligand with the key amino acids within the CDK2 active site Glu51, Leu83, Leu124, His125 and Asp145 (Figure 6).

As planned, the designed 3-(piperazinylmethyl)benzofuran derivatives adopted the common binding pattern of type II inhibitors. The thiosemicarbazide, semicarbazide, and acylhydrazone linker in benzofurans **9a-i**, **11a-e**, and **13a-c**, **15a,b** and **17**, respectively, are accommodated in the interface between the gate area and the allosteric back pocket in the kinase binding site interacting through hydrogen bonding with N-lobe α C helix Glu51 sidechain carboxylate and the DFG Asp145 backbone NH (Figures 7–9). From one side, this binding mode directs the peripheral (un)substituted phenyl moiety towards the hydrophobic region between the gate area and the hinge region interacting through hydrophobic interactions with the hydrophobic side chains of the surrounding Ala31, Val18, Val64, Phe80, Leu83, Leu134, Phe146 amino acids.

On the other side, the benzofuran ring is directed towards the hydrophobic allosteric back pocket interacting through hydrophobic interactions with the hydrophobic side chains of the amino

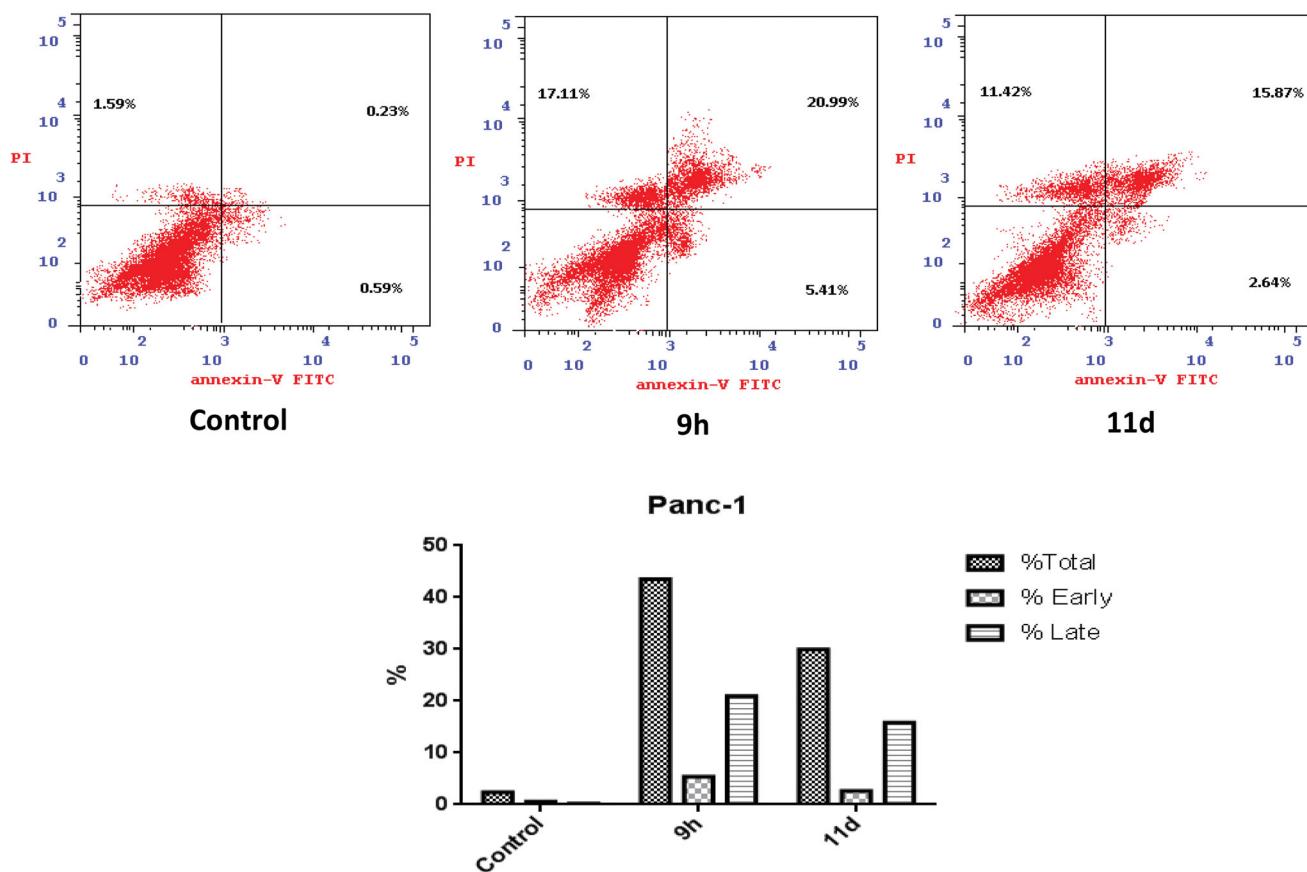
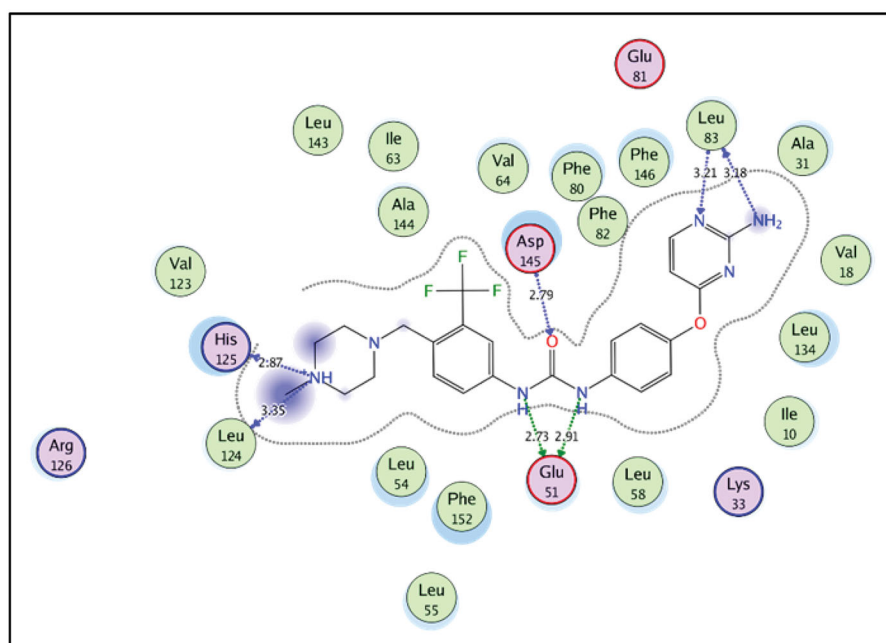
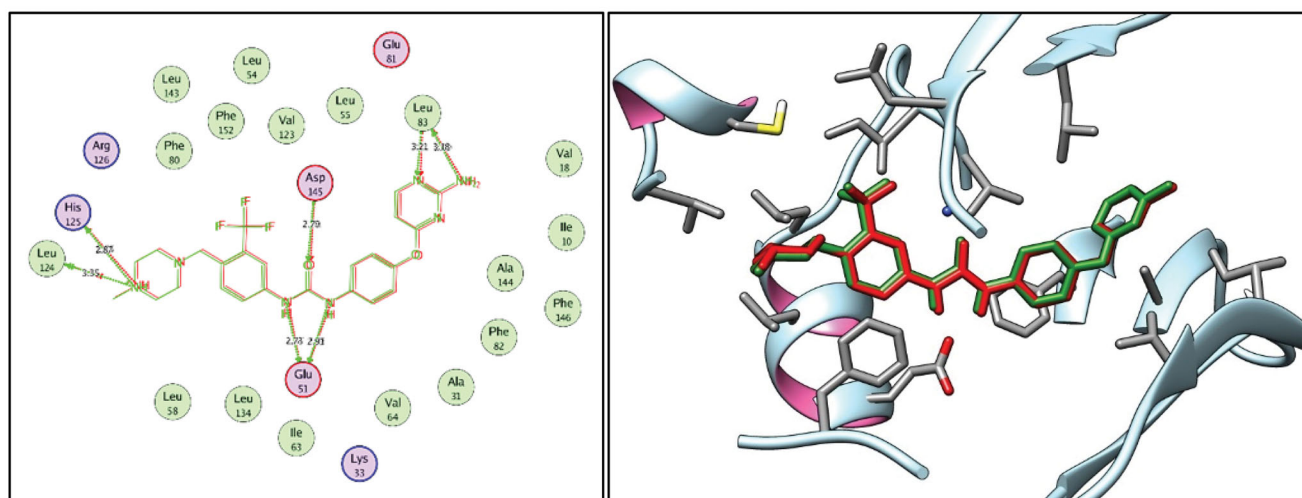


Figure 5. Influence of **9h** and **11d** on the percentage of annexin V-FITC-positive staining in Panc-1 cells.



(A)



(B)

(C)

Figure 6. (A) 2D interactions of compound I within the CDK2 active site. (B) and (C) 2D and 3D diagrams for the superimposition of the docking pose (green) and the co-crystallised pose (red) for compound I within the CDK2 binding site (RMSD = 0.245 Å).

acids lining the back pocket; Ala144, Phe152, and Leu55, besides, its π - π stacking interaction with Phe152 side chain. In addition, the phenylpiperazine moiety at 3-position of the benzofuran ring is extended towards a hydrophobic region surrounded by the hydrophobic side chains of the amino acids Leu54, Leu58, Ile63, Cys118, Val123, and Leu143.

3. Conclusions

In this study, different series of novel CDK2 type II inhibitors were designed *via* the hybridisation strategy between the privileged building blocks, benzofuran and piperazine, that were linked to different aromatic semicarbazide, thiosemicarbazide, or acylhydrazone tails to anchor the designed inhibitors onto the CDK2 kinase domain. The designed compounds showed promising CDK2

inhibitory activity with compounds **9h**, **11d**, **11e** and **13c** showing potent inhibitory activity (IC_{50} of 40.91, 41.70, 46.88, and 52.63 nM, respectively) compared to the used reference standard, staurosporine (IC_{50} of 56.76 nM). Moreover, the designed benzofurans showed promising cytotoxic activities with counterparts **9e**, **9h**, **11d**, and **13b** showing potent antiproliferative activity in agreement with their potent CDK2 inhibitory activity. Compound **9h** showed the most potent cytotoxic activity with IC_{50} of 0.94, 2.92, and 1.71 μ M against Panc-1, MCF-7, and A-549 cancer cell lines, respectively, in comparison to the used reference standard, cisplatin, (IC_{50} of 6.98, 5.45, and 6.72 μ M, respectively). On the other hand, the most potent compounds **9e**, **9h**, **11d**, and **13b** showed IC_{50} of 52.00, 27.70, 74.00 and 18.10 μ M, respectively, on normal lung fibroblasts (MRC-5 cell line) which represent SI of 9.92, 16.20, 24.75 and 10.58, respectively. These results indicate that these compounds are not only with promising CDK2 inhibitory activity

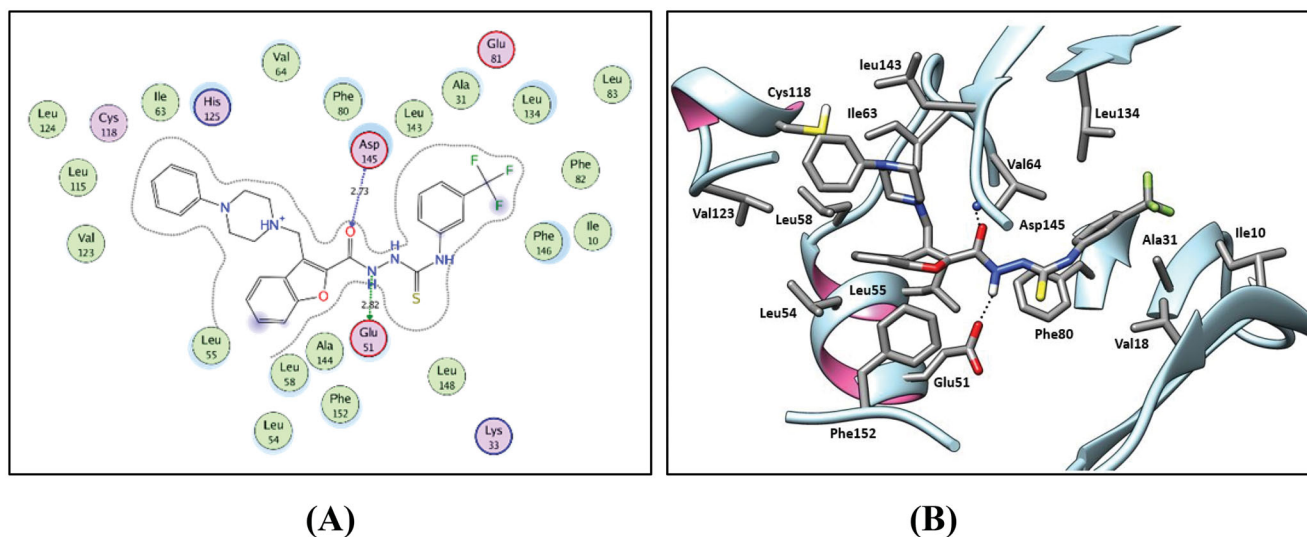


Figure 7. 2D diagram (A) and 3D representation (B) for the thiosemicarbazide derivative **9h** displaying its interaction within the CDK2 binding site.

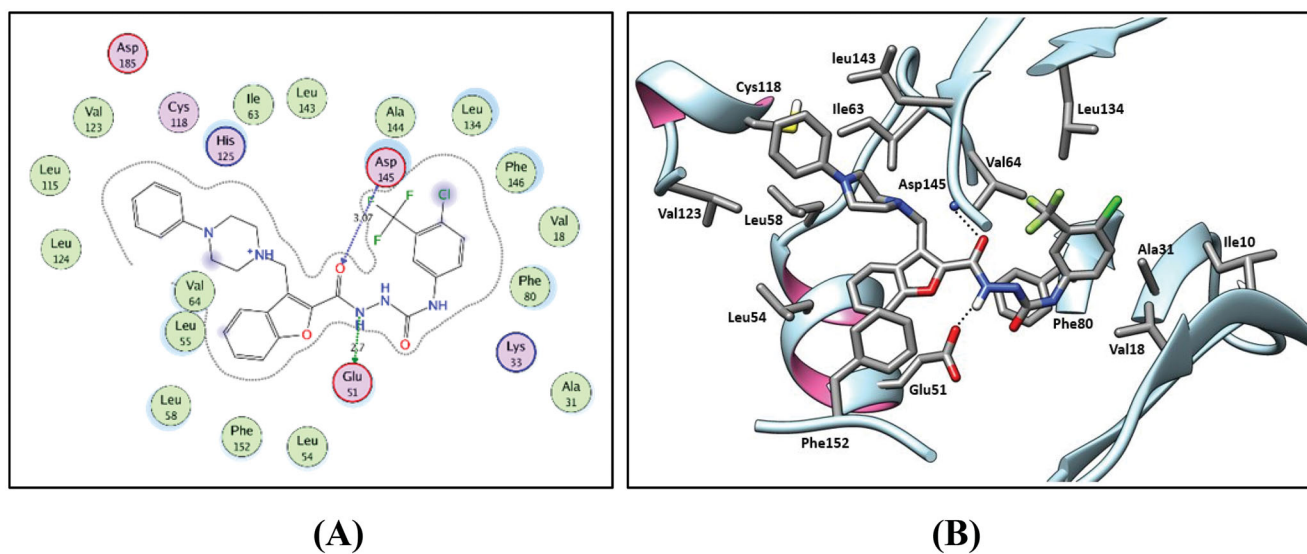


Figure 8. 2D diagram (A) and 3D representation (B) for the semicarbazide derivative **11d** displaying its interaction within the CDK2 binding site.

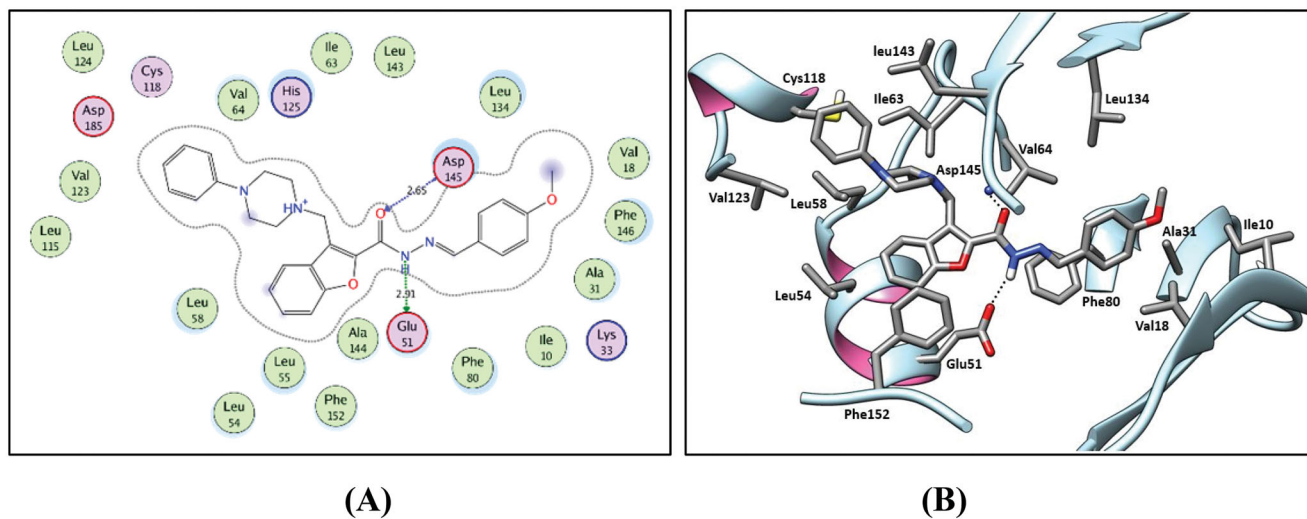


Figure 9. 2D diagram (A) and 3D representation (B) for the acylhydrazone derivative **13c** displaying its interaction within the CDK2 binding site.

and cytotoxicity but also with selectivity towards cancerous cells and so with tolerable and safe effect on normal cells. Cell cycle progression analysis of Panc-1 cell line using the most potent compounds **9h** and **11d** indicated that the newly synthesised compounds cause cell cycle arrest in the G2/M phase which is the main criterion of CDK2 inhibitors confirming the mode of action under investigation. Annexin V-FITC apoptosis assay on Panc-1 cell line using the most potent benzofurans **9h** and **11d** showed that the cell death resulted from the antiproliferative impact of the designed compounds is due to the physiological apoptosis and not due to a non-specific necrosis. Molecular docking simulations showed that, as planned, the designed compounds adopted the common binding pattern of type II inhibitors. The thiosemicarbazide, semicarbazide, and acylhydrazone linkers are accommodated in the interface between the gate area and the allosteric back pocket in the kinase binding site interacting through hydrogen bonding with N-lobe α C helix Glu51 side chain carboxylate and the DFG Asp145 backbone NH. From one side, this binding mode directs the peripheral (un)substituted phenyl moiety towards the hydrophobic region between the gate area and the hinge region, and on the other side, the benzofuran ring is directed towards the hydrophobic allosteric back pocket interacting through hydrophobic interactions with the hydrophobic side chains of the amino acids lining the back pocket. In addition, the phenylpiperazine moiety at 3-position of the benzofuran ring is extended towards a hydrophobic region surrounded by the hydrophobic side chains of the amino acids Leu54, Leu58, Ile63, Cys118, Val123, and Leu143.

4. Experimental

5.1. Materials and methods

Solvents, reagents and fine chemicals were purchased from Alfa Aesar and Sigma-Aldrich, and were used any without further purification. The NMR spectra were determined by Bruker 400 MHz spectrometer, and ^{13}C NMR spectra were run at 100 MHz in DMSO- d_6 . FLASH 2000 CHNS/O analyser, Thermo Scientific, was used for elemental analyses.

5.1.2. Preparation of ethyl 3-oxo-2-phenoxybutanoate (**3**)

Compound **3** was prepared as previously described⁸³.

5.1.3. Preparation of ethyl 3-methylbenzofuran-2-carboxylate (**4**)

The ester **3** (2.5 g, 11.3 mmol) was treated with sulphuric acid in ice-cooled flask 0–5 °C while stirring for 2h. After that, the mixture was added carefully to distilled water while stirring. Then, the benzofuran derivative (**4**) was extracted from the aqueous layer by DCM (3 × 12 ml). The combined organic extracts were washed once with equal volume of 10% aqueous NaHCO₃ solution then once again with water, and then finally it was dried over anhydrous magnesium sulphate. The residue after solvent evaporation was then recrystallized from methyl alcohol to afford 1.78 gm (77% yield) of white crystals of compound (**4**). The product melts at 49–51 °C, which confirmed its structure by matching with the reported one (48–50 °C)⁸⁴.

5.1.4. Preparation of ethyl 3-(bromomethyl)benzofuran-2-carboxylate (**5**)

Compound **4** (1.6 g, 8 mmol) was stirred with *N*-bromosuccinimide (NBS) (1.42 g, 8 mmol) in refluxing carbon tetrachloride for 3h. The

whole apparatus for this experiment was placed in a well-ventilated fume hood. At the end, the solvent was distilled off and the residue was re-dissolved in hot methyl alcohol to make a saturated solution. Then, the bromo derivative (**5**) was left to crystallise to afford 1.9 g (85% yield), m.p = 87–89 °C (reported⁸⁵ m.p = 86–87 °C).

5.1.5. Preparation of ethyl 3-((4-phenylpiperazin-1-yl)methyl)benzofuran-2-carboxylate (**6**)

The ester **5** (1.7 g, 6 mmol) was treated with *N*-phenylpiperazine reagent (1.05 g, 6.5 mmol) in the presence of catalytic amount of potassium iodide and potassium carbonate (1.80 g, 13 mmol) as a base. Acetone was used as solvent and the stirred reaction mixture was refluxed for 4h. After that, acetone was evaporated and the residue was triturated in 20 ml of cold water, stirred for 30 min, and then crystallised from ethanol 95% to produce compound **6** as white crystals, m.p = 140–141 °C, yield = 1.97 g, 90% of theoretical. The structure of compound **6** was further confirmed by ^1H NMR (400-MHz, DMSO- d_6): δ 8.07 (d, J = 7.9 Hz, 1H, Ar-H at C4 of benzofuran ring), 7.72 (d, J = 8.3 Hz, 1H, Ar-H at C7 of benzofuran ring), 7.55 (t, J = 7.6 Hz, 1H, Ar-H at C6 of benzofuran ring), 7.39 (t, J = 7.4 Hz, 1H, Ar-H at C5 of benzofuran ring), 7.21 (t, J = 7.4 Hz, 2H, two Ar-H at C3,5 phenyl), 6.92 (d, J = 7.9 Hz, 2H, two Ar-H at C2,6 phenyl), 6.78 (t, J = 7.2 Hz, 1H, one Ar-H at C4 phenyl), 4.40 (q, J = 7.0 Hz, 2H, methylene of CH_2CH_3), 4.10 (s, 2H, methylene exocyclic to C3 of benzofuran ring), 3.13 (s, 4H, two CH_2N piperazine moiety), 2.62 (s, 4H, two CH_2N piperazine moiety), 1.39 (t, J = 7.0 Hz, 3H, methyl of CH_2CH_3).

5.1.6. Preparation of 3-((4-phenylpiperazin-1-yl)methyl)benzofuran-2-carbohydrazide (**7**)

The ester **6** (2 g, 5.5 mmol) was dissolved in 20 ml of absolute ethanol then (1.1 ml, 22 mmol) of hydrazine hydrate (99%) was added portionwise while stirring at ambient temperature. Then, the whole reaction mixture was heated at reflux for 4h. After that, ethanols as well as most of hydrazine hydrate were evaporated under vacuum using rotavap. The remaining residue was then washed thoroughly for several times with distilled water while vigorous stirring then decantation after each time. Finally, the residue was crystallised from hot ethanol 80% to afford the hydrazide **7** as white crystals, m.p = 243–244 °C, yield = 1.41 g, 73% of theoretical. The structure of the hydrazide **7** was further confirmed by ^1H NMR. The product was used then in the next steps without further purification. ^1H NMR (400-MHz, DMSO- d_6) δ 10.68 (s, 1H, NH hydrazide), 7.97 (d, J = 7.8 Hz, 1H, Ar-H at C4 of benzofuran ring), 7.66 (d, J = 8.3 Hz, 1H, Ar-H at C7 of benzofuran ring), 7.49 (t, J = 7.6 Hz, 1H, Ar-H at C6 of benzofuran ring), 7.37 (t, J = 7.4 Hz, 1H, Ar-H at C5 of benzofuran ring), 7.23 (t, J = 7.5 Hz, 2H, two Ar-H at C3,5 phenyl), 6.94 (d, J = 7.9 Hz, 2H, two Ar-H at C2,6 phenyl), 6.80 (t, J = 7.1 Hz, 1H, one Ar-H at C4 phenyl), 4.66 (s, 2H, NH₂ hydrazide), 4.06 (s, 2H, methylene at C3 of benzofuran ring), 3.17 (s, 4H, two CH_2N piperazine moiety), 2.65 (s, 4H, two CH_2N piperazine moiety).

5.1.7. General method for the synthesis of thiosemicarbazides **9a-i** and semicarbazides **11a-e**

The hydrazide **7** (0.12 g, 0.34 mmol) and the appropriate derivative of isothiocyanates (**8a-i**, 0.4 mmol) or isocyanate (**10a-e**, 0.4 mmol) (0.4 mmol) were dissolved in hot stirred dry toluene (5 ml). After complete dissolution, the mixture was heated at reflux for 7h. Then, the produced precipitate was filtered by suction, air dried

and recrystallized from hot dioxane-toluene mixture (1:5, respectively) to afford the final thiosemicarbazides **9a-i** or semicarbazides **11a-e**, respectively (Full characterisation data are provided in the Supporting Information).

5.1.8. General procedure for the synthesis of hydrazone derivatives **13a-c**, **15a,b** and **17**:

The hydrazide **7** (0.12 g, 0.34 mmol) was dissolved in 10 ml of absolute ethanol. Then, the appropriate derivative of the aldehydes **12a-c** or the ketones **14a, b** or **16** (0.38 mmol) was added while stirring till clear solution was obtained. A few drops of acetic acid were added as a catalyst, then the whole reaction mixture was heated at reflux for 11h. After that, the reaction mixture was allowed to cool down to ambient temperature before being poured into a beaker containing 000 gm of crushed ice while stirring. The formed precipitate was allowed to settle down, and then filtered by suction, washed with water and air dried. Recrystallization from ethanol 80% afforded the final hydrazone derivatives **13a-c**, **15a,b** and **17** (Full characterisation data are provided in the Supporting Information).

5.2. Biological assays

The experimental details for the performed biological assays; Sulforhodamine B (SRB) cytotoxicity, CDK2 kinase, Annexin V-FITC apoptosis, and cell cycle assays^{86–89} were mentioned in the Supporting Information.

5.3. Molecular docking study

The experimental details of the adopted protocol, as well as its validation, for the molecular docking simulations were explained in the Supporting Information.

Disclosure statement

The authors declare that they have no known competing financial interests or personal relationships that could have appeared to influence the work reported in this paper.

Funding

The authors extend their appreciation to the Princess Nourah bint Abdulrahman University Researchers Supporting Project number (PNURSP2022R25), Princess Nourah bint Abdulrahman University, Riyadh, Saudi Arabia. The authors thank the Deanship of Scientific Research at Umm Al-Qura University for supporting this work by Grant Code: (22UQU4290565DSR010).

References

- American Cancer Society. Cancer facts & figures. 2020.
- Manning G, Whyte DB, Martinez R, et al. The protein kinase complement of the human genome. *Science* 2002;298:1912–34.
- Parang K, G, Sun Protein kinase inhibitors drug discovery. In: Gad SC ed. *Drug discovery handbook*. Hoboken, NJ: John Wiley & Sons, Inc.; 2005:1191–1257.
- Roskoski R. Jr, Classification of small molecule protein kinase inhibitors based upon the structures of their drug-enzyme complexes. *Pharmacol Res* 2016;103:26–48.
- Allam HA, Aly EE, Farouk A, et al. Design and Synthesis of some new 2,4,6-trisubstituted quinazoline EGFR inhibitors as targeted anticancer agents. *Bioorg Chem* 2020;98:103726.
- Al-Sanea MM, Elkamhawy A, Paik S, et al. Sulfonamide-based 4-anilinoquinoline derivatives as novel dual Aurora kinase (AURKA/B) inhibitors: Synthesis, biological evaluation and in silico insights. *Bioorg Med Chem* 2020;28:115525.
- Alonso A, Sasin J, Bottini N, et al. Protein tyrosine phosphatases in the human genome. *Cell* 2004;117:699–711.
- Bononi A, Agnoletto C, De Marchi E, et al. Protein kinases and phosphatases in the control of cell fate. *Enzyme Res* 2011;2011:329098.
- Zhang J, Yang PL, Gray NS. Targeting cancer with small molecule kinase inhibitors. *Nat Rev Cancer* 2009;9:28–39.
- Fabbro D, Ruetz S, Buchdunger E, et al. Protein kinases as targets for anticancer agents: from inhibitors to useful drugs. *Pharmacol Ther* 2002;93:79–98.
- Pearson M, C, García-Echeverría, D, Fabbro Protein tyrosine kinases as targets for cancer and other indications. In: Fabbro D, Mc Cormick F, eds. *Protein tyrosine kinases – From Inhibitors to Useful Drugs*. Totowa, NJ: Humana Press Inc.; 2006:1–29.
- Sedlacek HH. Kinase inhibitors in cancer therapy: a look ahead. *Drugs* 2000;59:435–76.
- Weinstein IB, Joe AK. Mechanisms of disease: Oncogene addiction-a rationale for molecular targeting in cancer therapy. *Nat Clin Pract Oncol* 2006;3:448–57.
- Padma VV. An overview of targeted cancer therapy. *BioMedicine* 2015;5:19.
- Aggarwal S. Targeted cancer therapies. *Nat Rev Drug Discov* 2010;9:427–8.
- Topcul M, Cetin I. Endpoint of cancer treatment: targeted therapies. *Asian Pac J Cancer Prev* 2014;15:4395–403.
- Malumbres M. Physiological relevance of cell cycle kinases. *Physiol Rev* 2011;91:973–1007.
- Malumbres M, Barbacid M. Mammalian cyclin-dependent kinases. *Trends Biochem Sci* 2005;30:630–41.
- Lapenna S, Giordano A. Cell cycle kinases as therapeutic targets for cancer. *Nat Rev Drug Discov* 2009;8:547–66.
- Asghar U, Witkiewicz AK, Turner NC, Knudsen ES. The history and future of targeting cyclin-dependent kinases in cancer therapy. *Nat Rev Drug Discov* 2015;14:130–46.
- Horiuchi D, Huskey NE, Kusdra L, et al. Chemical-genetic analysis of cyclin dependent kinase 2 function reveals an important role in cellular transformation by multiple oncogenic pathways. *Proc Natl Acad Sci USA* 2012;109:E1019–1027.
- He X, Xiang H, Zong X, et al. CDK2-AP1 inhibits growth of breast cancer cells by regulating cell cycle and increasing docetaxel sensitivity in vivo and in vitro. *Cancer Cell Int* 2014;14:130.
- Alexander A, Karakas C, Chen X, et al. Cyclin E overexpression as a biomarker for combination treatment strategies in inflammatory breast cancer. *Oncotarget* 2017;8:14897–911.
- Ding L, Cao J, Lin W, et al. The Roles of Cyclin-Dependent Kinases in Cell-Cycle Progression and Therapeutic Strategies in Human Breast Cancer. *Int J Mol Sci* 2020;21(6):1960.
- Harwell RM, Porter DC, Danes C, Keyomarsi K. Processing of cyclin E differs between normal and tumor breast cells. *Cancer Res* 2000;60:481–9.
- Cooley A, Zelivianski S, Jeruss JS. Impact of cyclin E overexpression on Smad3 activity in breast cancer cell lines. *Cell Cycle* 2010;9:4900–7.

27. Luk KC, Simcox ME, Schutt A, et al. A new series of potent oxindole inhibitors of CDK2. *Bioorg Med Chem Lett* 2004;14: 913–7.
28. Chohan TA, Qayyum A, Rehman K, et al. An insight into the emerging role of cyclin-dependent kinase inhibitors as potential therapeutic agents for the treatment of advanced cancers. *Biomed Pharmacother* 2018;107:1326–41.
29. Chohan TA, Qian H, Pan Y, Chen JZ. Cyclin-dependent kinase-2 as a target for cancer therapy: progress in the development of CDK2 inhibitors as anti-cancer agents. *Curr Med Chem* 2015;22:237–63.
30. Abd El-Karim SS, Syam YM, El Kerdawy AM, Abdelghany TM. New thiazol-hydrazono-coumarin hybrids targeting human cervical cancer cells: Synthesis, CDK2 inhibition, QSAR and molecular docking studies. *Bioorg Chem* 2019;86:80–96.
31. Marak BN, Dowarah J, Khiangte L, Singh VP. A comprehensive insight on the recent development of Cyclic Dependent Kinase inhibitors as anticancer agents. *Eur J Med Chem* 2020;203:112571.
32. Ali S, Heathcote DA, Kroll SH, et al. The development of a selective cyclin-dependent kinase inhibitor that shows anti-tumor activity. *Cancer Res* 2009;69:6208–15.
33. Węsierska-Gądek J, Gritsch D, Zulehner N, et al. Roscovitine, a selective CDK inhibitor, reduces the basal and estrogen-induced phosphorylation of ER- α in human ER-positive breast cancer cells. *J Cell Biochem* 2011;112:761–72.
34. Johnson N, Bentley J, Wang LZ, et al. Pre-clinical evaluation of cyclin-dependent kinase 2 and 1 inhibition in anti-estrogen-sensitive and resistant breast cancer cells. *Br J Cancer* 2010;102:342–50.
35. Alexander LT, Mobitz H, Druceckes P, et al. Type II Inhibitors Targeting CDK2. *ACS Chem Biol* 2015;10:2116–25.
36. Liu Y, Gray NS. Rational design of inhibitors that bind to inactive kinase conformations. *Nature Chemical Biology* 2006;2:358–64.
37. Eldehna WM, Abou-Seri SM, El Kerdawy AM, et al. Increasing the binding affinity of VEGFR-2 inhibitors by extending their hydrophobic interaction with the active site: Design, synthesis and biological evaluation of 1-substituted-4-(4-methoxybenzyl)phthalazine derivatives. *Eur J Med Chem* 2016;113: 50–62.
38. Eldehna WM, El Kerdawy AM, Al-Ansary GH, et al. Type IIA - Type IIB protein tyrosine kinase inhibitors hybridization as an efficient approach for potent multikinase inhibitor development: Design, synthesis, anti-proliferative activity, multikinase inhibitory activity and molecular modeling of novel indolinone-based ureides and amides. *Eur J Med Chem* 2019;163:37–53.
39. Broekman F, Giovannetti E, Peters GJ. Tyrosine kinase inhibitors: Multi-targeted or single-targeted? *World J Clin Oncol* 2011;2:80–93.
40. Cheng W, Yang Z, Wang S, et al. Recent development of CDK inhibitors: An overview of CDK/inhibitor co-crystal structures. *Eur J Med Chem* 2019;164:615–39.
41. H. KhanamShamsuzzaman Bioactive Benzofuran derivatives: A review. *Eur J Med Chem* 2015;97:483–504.
42. Miao Y-h, Hu Y-h, Yang J, et al. Natural source, bioactivity and synthesis of benzofuran derivatives. *RSC Adv* 2019;9: 27510–40.
43. Hassan GS, Georgey HH, George RF, Mohamed ER. Aurones and furoaurones: Biological activities and synthesis. *Bull Fac Pharm Cairo Univ* 2018;56:121–7.
44. Eldehna WM, Al-Rashood ST, Al-War-Hi T, et al. Novel oxindole/benzofuran hybrids as potential dual CDK2/GSK-3 β inhibitors targeting breast cancer: design, synthesis, biological evaluation, and in silico studies. *J Enzyme Inhib Med Chem* 2021;36:270–85.
45. Eldehna WM, Nocentini A, Elsayed ZM, et al. Benzofuran-Based Carboxylic Acids as Carbonic Anhydrase Inhibitors and Antiproliferative Agents against Breast Cancer. *ACS Med Chem Lett* 2020;11:1022–7.
46. Gaisina IN, Gallier F, Ougolkov AV, et al. From a natural product lead to the identification of potent and selective benzofuran-3-yl-(indol-3-yl)maleimides as glycogen synthase kinase 3 β inhibitors that suppress proliferation and survival of pancreatic cancer cells. *J Med Chem* 2009;52: 1853–63.
47. Salomé C, Narbonne V, Ribeiro N, et al. Benzofuran derivatives as a novel class of inhibitors of mTOR signaling. *Euro J Med Chem* 2014;74:41–9.
48. Salomé C, Ribeiro N, Chavagnan T, et al. Benzofuran derivatives as anticancer inhibitors of mTOR signaling. *Euro J Med Chem* 2014;81:181–91.
49. Xiang Y, Hirth B, Asmussen G, et al. The discovery of novel benzofuran-2-carboxylic acids as potent Pim-1 inhibitors. *Bioorg Med Chem Lett* 2011;21:3050–6.
50. Abd El-Karim SS, Anwar MM, Mohamed NA, et al. Design, synthesis, biological evaluation and molecular docking studies of novel benzofuran-pyrazole derivatives as anticancer agents. *Bioorg Chem* 2015;63:1–12.
51. Finlay MR, Acton DG, Andrews DM, et al. Imidazole piperazines: SAR and development of a potent class of cyclin-dependent kinase inhibitors with a novel binding mode. *Bioorg Med Chem Lett* 2008;18:4442–6.
52. Ananda Kumar CS, Benaka Prasad SB, Vinaya K, et al. Synthesis and in vitro antiproliferative activity of novel 1-benzhydrylpiperazine derivatives against human cancer cell lines. *Eur J Med Chem* 2009;44:1223–9.
53. WALAYAT K, MOHSIN N-u-A, ASLAM S, AHMAD M. An insight into the therapeutic potential of piperazine-based anticancer agents. *Turk J Chem* 2019;43:1–23.
54. Chen P, Lee NV, Hu W, et al. Spectrum and Degree of CDK Drug Interactions Predicts Clinical Performance. *Mol Cancer Ther* 2016;15:2273–81.
55. Shaquiquzzaman M, Verma G, Marella A, et al. Piperazine scaffold: A remarkable tool in generation of diverse pharmacological agents. *Eur J Med Chem* 2015;102:487–529.
56. Rathi AK, Syed R, Shin HS, Patel RV. Piperazine derivatives for therapeutic use: a patent review (2010-present). *Expert Opin Ther Pat* 2016;26:777–97.
57. Yu Z, Wang R, Xu L, et al. β -Elemene piperazine derivatives induce apoptosis in human leukemia cells through downregulation of c-FLIP and generation of ROS. *PLoS One* 2011;6: e15843.
58. Vianello P, Botrugno OA, Cappa A, et al. Discovery of a novel inhibitor of histone lysine-specific demethylase 1A (KDM1A/LSD1) as orally active antitumor agent. *J Med Chem* 2016;59:1501–17.
59. Chung KS, Han G, Kim BK, et al. A novel antitumor piperazine alkyl compound causes apoptosis by inducing RhoB expression via ROS-mediated c- Abl/p38 MAPK signaling. *Cancer Chemother Pharmacol* 2013;72:1315–24.
60. Torrente E, Parodi C, Ercolani L, et al. Synthesis and in Vitro Anticancer Activity of the First Class of Dual Inhibitors of REV-ERB β and Autophagy. *J Med Chem* 2015;58:5900–15.

61. Chetan B, Bunha M, Jagrat M, et al. Design, synthesis and anticancer activity of piperazine hydroxamates and their histone deacetylase (HDAC) inhibitory activity. *Bioorg Med Chem Lett* 2010;20:3906–10.
62. Sharath Kumar KS, Hanumappa A, Hegde M, et al. Synthesis and antiproliferative effect of novel 4-thiazolidinone-, pyridine- and piperazine-based conjugates on human leukemic cells. *Eur J Med Chem* 2014;81:341–9.
63. Arnatt CK, Adams JL, Zhang Z, et al. Design, syntheses, and characterization of piperazine based chemokine receptor CCR5 antagonists as anti prostate cancer agents. *Bioorg Med Chem Lett* 2014;24:2319–23.
64. Wang KR, Qian F, Sun Q, et al. Substituent Effects on Cytotoxic Activity, Spectroscopic Property, and DNA Binding Property of Naphthalimide Derivatives. *Chem Biol Drug Des* 2016;87:664–72.
65. Dessole G, JONES P, BUFI L, et al. 1,2,4-oxadiazole substituted piperidine and piperazine derivatives as SMO Antagonists - WO/2010/013037. 2010.
66. Jones P, Ontoria JM. Piperidine and piperazine derivatives as SMO Antagonists - WO/2011/036478. 2011.
67. FAJAS L, BENFODDA Z, FRITZ V. Novel inhibitors of stearyl-coa-desaturase-1 and their uses - WO/2011/030312. 2011.
68. S, Wang, H, Zhou, J, Chen, et al., Bcl-2/bcl-xl inhibitors and therapeutic methods using the same - US20120189539A1. 2012.
69. Reiner T, Keliher EJ, Weissleder R. Compositions and methods for in vivo imaging - WO2012074840. 2012.
70. Rosell R, Gettinger SN, Bazhenova LA, et al. 1330: Brigatinib efficacy and safety in patients (Pts) with anaplastic lymphoma kinase (ALK)-positive (ALK+) non-small cell lung cancer (NSCLC) in a phase 1/2 trial. *J Thorac Oncol* 2016;11:S114.
71. Druker BJ. STI571 (Gleevec™) as a paradigm for cancer therapy. *Trends Mol Med* 2002;8:S14–S18.
72. De Falco V, Buonocore P, Muthu M, et al. Ponatinib (AP24534) is a novel potent inhibitor of oncogenic RET mutants associated with thyroid cancer. *J Clin Endocrinol Metab* 2013;98:E811–819.
73. Sequist LV, Soria JC, Goldman JW, et al. Rociletinib in EGFR-mutated non-small-cell lung cancer. *N Engl J Med* 2015;372:1700–9.
74. El-Miligy MM, Abd El Razik HA, Abu-Serie MM. Synthesis of piperazine-based thiazolidinones as VEGFR2 tyrosine kinase inhibitors inducing apoptosis. *Fut Med Chem* 2017;9:1709–29.
75. Sun J, Ren SZ, Lu XY, et al. Discovery of a series of 1,3,4-oxadiazole-2(3H)-thione derivatives containing piperazine skeleton as potential FAK inhibitors. *Bioorg Med Chem* 2017;25:2593–600.
76. Gao J, Fang C, Xiao Z, et al. Discovery of novel 5-fluoro-N2,N4-diphenylpyrimidine-2,4-diamines as potent inhibitors against CDK2 and CDK9. *Medchemcomm* 2015;6:444–54.
77. Hamilton E, Infante JR. Targeting CDK4/6 in patients with cancer. *Cancer Treat Rev* 2016;45:129–38.
78. Cherukupalli S, Chandrasekaran B, Krystof V, et al. Synthesis, anticancer evaluation, and molecular docking studies of some novel 4,6-disubstituted pyrazolo[3,4-d]pyrimidines as cyclin-dependent kinase 2 (CDK2) inhibitors. *Bioorg Chem* 2018;79:46–59.
79. Oakes V, Wang W, Harrington B, et al. Cyclin A/Cdk2 regulates Cdh1 and claspin during late S/G2 phase of the cell cycle. *Cell Cycle* 2014;13:3302–11.
80. Martin A, Odajima J, Hunt SL, et al. Cdk2 is dispensable for cell cycle inhibition and tumor suppression mediated by p27(Kip1) and p21(Cip1). *Cancer Cell* 2005;7:591–8.
81. Gorczyca W. Cytometric analyses to distinguish death processes. *Endocr Relat Cancer* 1999;6:17–9.
82. Mahajan P, Chashoo G, Gupta M, et al. Fusion of Structure and Ligand Based Methods for Identification of Novel CDK2 Inhibitors. *J Chem Inf Model* 2017;57:1957–69.
83. Shaldam M, Eldehna WM, Nocentini A, et al. Development of novel benzofuran-based SLC-0111 analogs as selective cancer-associated carbonic anhydrase isoform IX inhibitors. *Eur J Med Chem* 2021;216:113283.
84. Wasson BK, Hamel P, Rooney CS. A synthesis of 6-hydroxy-1-benzoxepin-3, 5 (2H, 4H)-dione. *J Org Chem* 1977;42:4265–6. no.
85. Coaviche-Yoval A, Luna H, Tovar-Miranda R, et al. Synthesis and biological evaluation of novel 2,3-disubstituted Benzofuran Analogues of GABA as Neurotropic Agents. *Med Chem* 2019;15:77–86.
86. Eldehna WM, El Hassab MA, Abo-Ashour MF, et al. Development of isatin-thiazolo[3,2-a]benzimidazole hybrids as novel CDK2 inhibitors with potent in vitro apoptotic anti-proliferative activity: Synthesis, biological and molecular dynamics investigations. *Bioorg. Chem* 2021;110:104748.
87. Eldehna W, Fares M, Ibrahim H, et al. Synthesis and cytotoxic activity of biphenylurea derivatives containing indolin-2-one moieties. *Molecules* 2016;21:762.
88. Abdel-Aziz HA, Ghabbour HA, Eldehna WM, et al. Synthesis, crystal structure, and biological activity of cis/trans amide rotomers of (Z)-N'-(2-oxoindolin-3-ylidene)formohydrazide. *J Chem* 2014;2014:1–7.
89. Sabt A, Eldehna WM, Al-Warhi T, et al. Discovery of 3,6-disubstituted pyridazines as a novel class of anticancer agents targeting cyclin-dependent kinase 2: synthesis, biological evaluation and in silico insights. *J Enzyme Inhib Med Chem* 2020;35:1616–30.